

A STRESS INTENSITY FACTOR SOLUTION INSPIRED BY SOAP BUBBLES FRAMEWORK

Raül de Moura Pinho, Didier Soria, Loïc Dimithe Aboumou

**Safran Aircraft Engines, Rond-point René Ravaud-Réau, 77550 Moissy-Cramayel
 raul.de-moura-pinho@safrangroup.com**

Keywords: *Stress Intensity Factor, shape functions, optimization algorithm, finite element method, soap bubbles mathematics*

Abstract

For the design of aircraft engines in service life it is helpful, in terms of computing time reduction, to perform simulations with simplified plane cracks geometries subjected to simple loads, often polynomial. This work focuses on a realistic method of estimating the stress intensity factor K_I based on the physics of the phenomenon.

The stress intensity factor solution is determined from finite elements simulations. For each crack geometry, for a given size of the plate in which the crack propagates and for a given stress field applied to the plate, the stress intensity factor is determined with a test matrix.

The aim of this paper is to give a methodology which leads to improve the interpolation of tabulated values of K_I so that it is more representative of the fracture mechanics. For this, a finite element based approach is used, but with shape functions more adapted to the fracture mechanics problem. The algorithm is inspired by soap bubbles mathematics.

1 Introduction

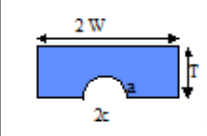
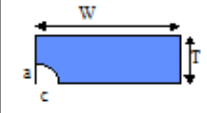
In this paper, we focus on an approach to determine quickly and accurately enough, the stress intensity factors from the data concerning the geometry of the propagation plane, loading applied to the propagation plane and geometry of the crack.

Before describing the outline of our methodology, let's introduce the Bueckner's principle [1, 2]. This principle makes equivalent the problem of the initial cracked structure (a) to the superposition of two other problems. The first (b) is identical to the original one except

that it contains no crack. In the second (c) the load is applied at the lips of the crack such that the superposition of the stress field induced by both problems leads to a zero load on the lips of the crack. The load applied on the lips of the crack in the problem (c) is the load which will be considered next. Moreover, the stress intensity factor of the problem (a) is equal to that of the problem (c) since that of the problem (b) is equal to zero.

Typically, engineers replace the original real cracking problem with a more simple to solve. For example, the crack geometry may be semi-elliptical or quarter-elliptical. Further simplification is to consider that the loading applied to the propagation plane can be represented with good accuracy by a polynomial stress field of degree 6 (bi- or mono-dimensional). More general approaches such as those on weight functions [3] will not be discussed here.

Several formulas for the stress intensity factor are used at Safran Aircraft Engines. Those that will interest us in this work are detailed in the following table:

Crack geometry	Stress gradient
Semi-elliptical 	1D
Quarter-elliptical 	2D

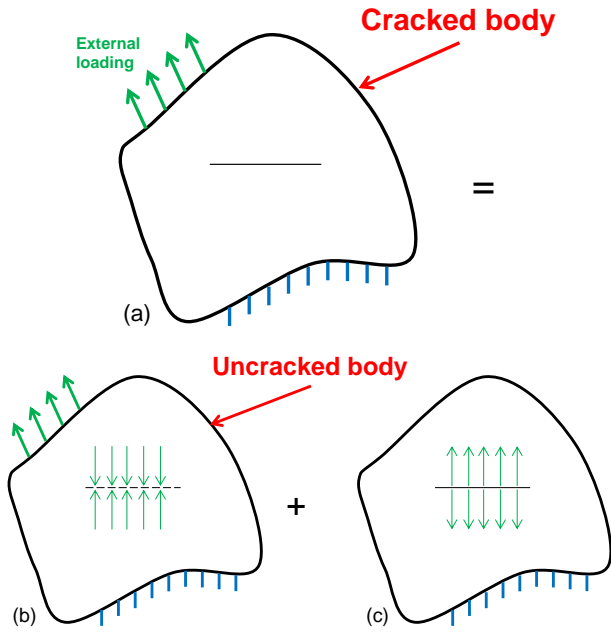


Fig. 1. Bueckner's principle.

Both stress intensity factor solutions were determined from numerical simulations by finite element method. For each crack geometry, for a given size of the crack plane and a stress field applied to the crack plane, giving a matrix of all cases to simulate the stress intensity factor was determined. The identification of the stress intensity factor solution is based on the following formula:

$$K_I = \sigma \cdot F_I \left(\frac{a}{T}, \frac{a}{c} \right) \cdot \frac{F_W}{E_k} \cdot \sqrt{\pi \cdot a} \quad (1)$$

Thus the $F_I \left(\frac{a}{T}, \frac{a}{c} \right)$ factor is determined for each of the numerical cases studied, with:

$$E_k = \begin{cases} \sqrt{1 + 4,464 \cdot \left(\frac{a}{c} \right)^{1,65}} & \text{if } a \leq c \\ \sqrt{1 + 4,464 \cdot \left(\frac{c}{a} \right)^{1,65}} & \text{else} \end{cases} \quad (2)$$

$$F_W = \frac{1}{\sqrt{\cos \left(\frac{\pi \cdot c \cdot \sqrt{\frac{a}{T}}}{W} \right)}} \quad (3)$$

The current method is to extrapolate $F_I \left(\frac{a}{T}, \frac{a}{c} \right)$ linearly between the discretized values in order to get a continuous field.

The work presented in this paper is to improve the previous interpolation so that it is more representative of the physics of the problem, thanks to the soap bubbles mathematics.

2 Numerical considerations

2.1 Analogy between a mesh and a grid data

For interpolation, a finite element approach is used, but with shape functions "adapted" to our problem. The discretization is now seen as a finite element mesh with quadrangular elements. In each node of the mesh, the $F_I \left(\frac{a}{T}, \frac{a}{c} \right)$ factor is known and its partial derivatives with respect to a/T and a/c have to be determined. The convention defined by the graph for the numbering of nodes for a given element will be adopted in the next.

In this approach all degrees of freedom are determined at the nodes defined by the discretization. An element of type C2-Q5 will be used (continuity of second partial derivatives in the element with polynomial shape functions of degree 5). 36 degrees of freedom are needed in order to transmit the regular property from the element scale to the mesh in its entirety [4]. Each node is associated with 9 degrees of freedom corresponding to the nodal values of the function $\Phi \left(x = \left(\frac{a}{T} \right)_{i \text{ reduced}}, y = \left(\frac{a}{c} \right)_{i \text{ reduced}} \right)$ (represent $F_I \left(\frac{a}{T}, \frac{a}{c} \right)$ and its derivatives in reduced coordinates).

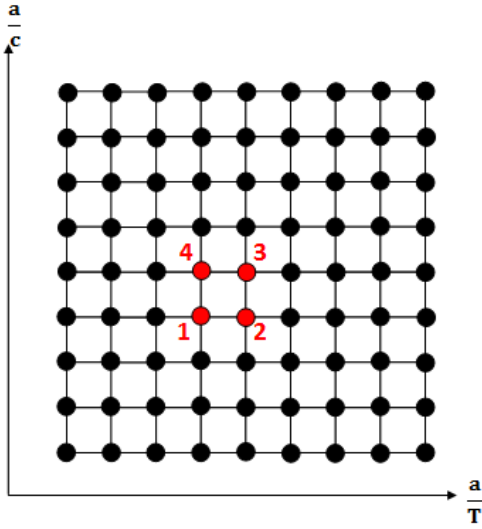


Fig. 2. Discretized values seen as a mesh.

2.2 1D shape functions

The 2D shape functions of this element are built from the following 1D polynomial shape functions:

$$\begin{cases} C_{1,1}(x) = 0,5 - 0,9375 \cdot x \\ \quad \quad \quad + 0,625 \cdot x^3 - 0,1875 \cdot x^5 \\ C_{1,2}(x) = 0,3125 - 0,4375 \cdot x - 0,375 \cdot x^2 \\ \quad \quad \quad + 0,625 \cdot x^3 + 0,0625 \cdot x^4 - 0,1875 \cdot x^5 \\ C_{1,3}(x) = 0,0625 - 0,0625 \cdot x - 0,125 \cdot x^2 \\ \quad \quad \quad + 0,125 \cdot x^3 + 0,0625 \cdot x^4 - 0,0625 \cdot x^5 \\ C_{2,1}(x) = 0,5 + 0,9375 \cdot x - 0,625 \cdot x^3 + 0,1875 \cdot x^5 \\ C_{2,2}(x) = -0,3125 - 0,4375 \cdot x + 0,375 \cdot x^2 \\ \quad \quad \quad + 0,625 \cdot x^3 - 0,0625 \cdot x^4 - 0,1875 \cdot x^5 \\ C_{2,3}(x) = 0,0625 + 0,0625 \cdot x - 0,125 \cdot x^2 \\ \quad \quad \quad - 0,125 \cdot x^3 + 0,0625 \cdot x^4 + 0,0625 \cdot x^5 \end{cases} \quad (4)$$

The first index indicates the node number on which the nodal value is taken.

The second index indicates the nature of the nodal value:

- **1** : nodal value of $\Phi \left(x = \left(\frac{a}{T} \right)_{i \text{ reduced}}, y = \left(\frac{a}{c} \right)_{i \text{ reduced}} \right)$
- **2** : nodal value of the derivative of $\Phi \left(x = \left(\frac{a}{T} \right)_{i \text{ reduced}}, y = \left(\frac{a}{c} \right)_{i \text{ reduced}} \right)$ with respect to x
- **3** : nodal value of the second derivative of $\Phi \left(x = \left(\frac{a}{T} \right)_{i \text{ reduced}}, y = \left(\frac{a}{c} \right)_{i \text{ reduced}} \right)$ with respect to x

The 1D element associated with these shape functions is defined so that the first node is located at $x = -1$ and the second at $x = 1$.

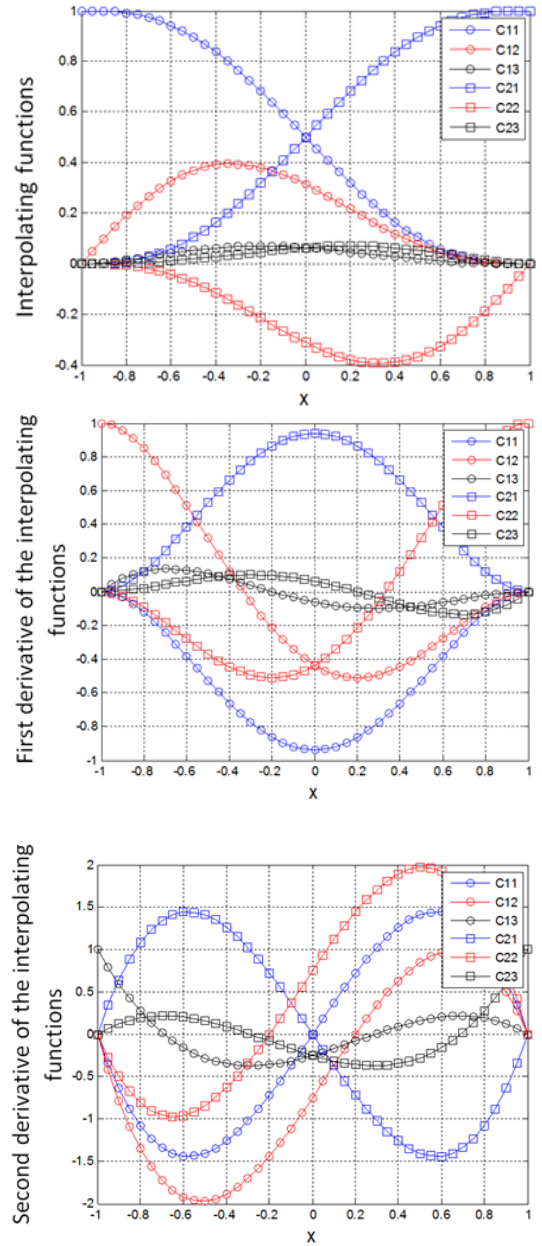


Fig. 3. 1D Interpolating functions and their derivatives.

2.3 2D shape functions

2D shape functions are products of the preceding elementary functions. The final interpolation is written as the dot product of two vectors, one of which contains all the necessary information regarding the computation of Φ at nodes.

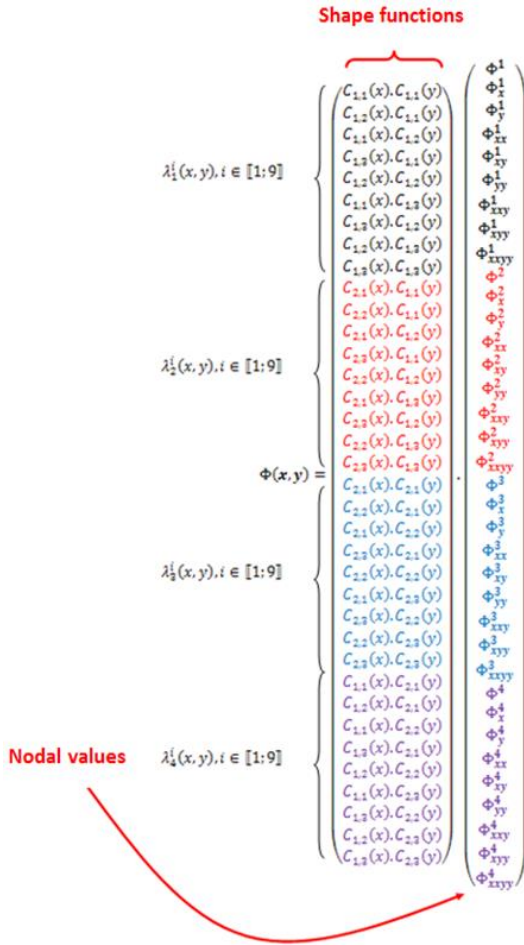


Fig. 4. Mathematical representation of Φ

The following notation is used for Φ , the top index is the node number for which the nodal value is given and the low index refers to variables against which the partial derivative is calculated. The reference element thus defined is square and its boundaries are the boundaries of the domain $[-1, 1] \times [-1, 1]$.

Here are some visualizations of 2D shape functions associated with the unit nodal values at the node 1. For other nodes, the shape functions are similar to those associated with the node 1.

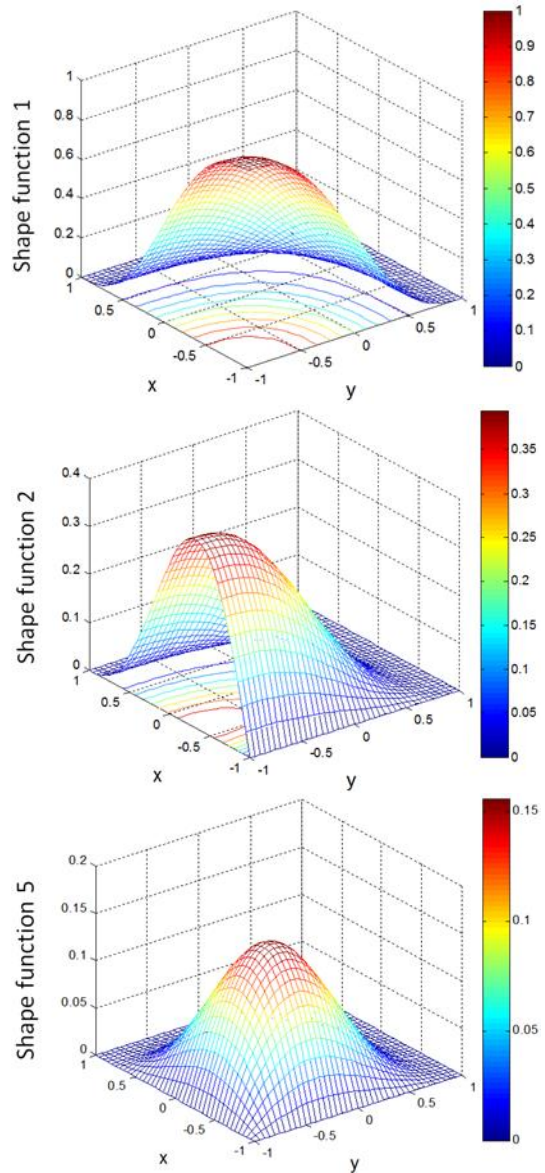


Fig. 5. Example of shape functions associated with the first node

2.4 Contributions of such an approach

When the test field associated with an element is equal to 1 with the derivatives equal to 0 at nodes:

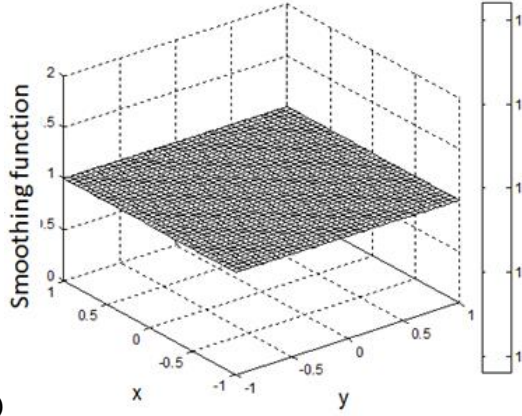
- A constant field is obtained as expected
- This is the result obtained with a linear interpolation as that used in the previous version of our tools.

When the test field and its derivatives are equal to 1 at nodes:

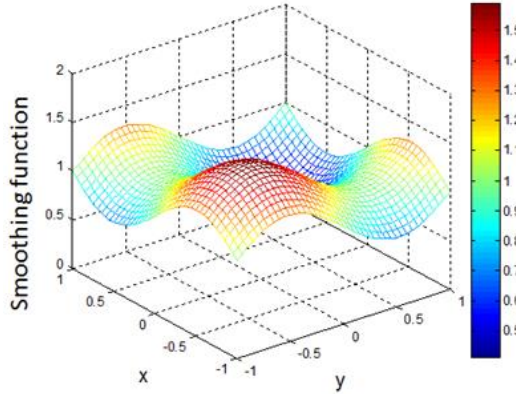
- Complex shape field
- The shape cannot be represented by a simple linear interpolation.

The advantages of this interpolation method:

- C2 regularity of Φ in the common boundary of two elements. This property is extended to the whole mesh.
- Possibility to calculate the curvatures on the surface (possibility to optimize the smoothing).



(a)



(b)

Fig. 6. Examples of smoothing functions:

- (a) case where the field values to the nodes are the same with derivatives equal to zero in the same nodes,
 (b) case where the field values and its derivatives to the nodes are the same.

2.5 Drawbacks of such an approach

Several numerical simulations were performed taking into account the distribution of discretized values of $\frac{a}{T}$ and $\frac{a}{c}$:

$$\begin{cases} \frac{a}{T} \in \{0,1; 0,2; 0,4; 0,6; 0,8\} \\ \frac{a}{c} \in \{0,1; 0,2; 0,4; 0,6; 0,8;\} \\ \quad \quad \quad \{1; 1,2; 1,5; 2; 5; 10\} \end{cases} \quad (5)$$

However, the results of this regular grid led to smoothing of the $F_I\left(\frac{a}{T}, \frac{a}{c}\right)$ factor with very pronounced spatial oscillations. The problem was not the code or the process, but the intervals defined by the discretization introduce scale effects induced by the different dimensions of

the elements. To solve this problem, we had to introduce a virtual mesh leading to the same dimension of the elements:

$$\begin{cases} \frac{a}{T_{virtual}} \in \{1; 2; 3; 4; 5\} \\ \frac{a}{c_{virtual}} \in \{1; 2; 3; 4; 5; 6;\} \\ \quad \quad \quad \{7; 8; 9; 10; 11\} \end{cases} \quad (6)$$

In the next section $\frac{a}{T}$ is designate instead of $\frac{a}{T_{virtual}}$ and $\frac{a}{c}$ instead of $\frac{a}{c_{virtual}}$. The transition from virtual to real mesh will be specified soon.

3 Operating soap bubbles mathematics

3.1 Mesh with only one element

The aim is to get a smooth surface through the discretized values of the $F_I\left(\frac{a}{T}, \frac{a}{c}\right)$ factor to the nodes of the element. The element selected is of kind C2-Q5, which implies that smoothing is regular. However, to obtain the most natural surface, one possibility is to minimize the surface of the smoothing and the local curvatures induced. The following functional is proposed:

$$J_{elem} = \iint_{S_{elem}} \mu(u, v) \cdot \Omega(u, v) \cdot du \cdot dv, \quad (7)$$

with $u = \frac{a}{T}$ et $v = \frac{a}{c}$

To understand the different terms in this expression, some recalls of differential geometry are presented. The infinitesimal volume element can be written from the coefficients of the first fundamental form characterizing the surface. Thus:

$$dS = \sqrt{E\left(\frac{a}{T}, \frac{a}{c}\right) \cdot G\left(\frac{a}{T}, \frac{a}{c}\right) - F\left(\frac{a}{T}, \frac{a}{c}\right)^2} \cdot d\left(\frac{a}{T}\right) \cdot d\left(\frac{a}{c}\right) \quad (8)$$

$$\text{with } \mu\left(\frac{a}{T}, \frac{a}{c}\right) = \sqrt{E\left(\frac{a}{T}, \frac{a}{c}\right) \cdot G\left(\frac{a}{T}, \frac{a}{c}\right) - F\left(\frac{a}{T}, \frac{a}{c}\right)^2}.$$

From the second fundamental form (coefficients H and K), the mean square radius is defined by:

$$\Omega = \frac{k_1^2 + k_2^2}{2} = 2 \cdot H^2 - K \quad (9)$$

So J_{elem} can be seen as a kind of curvature energy that is to be minimized. The link with the physics of soap bubbles is thus cleared.

Indeed, the geometry of a soap bubble can be deduced from a problem of energy minimization quite similar to that which has just been stated.

3.2 Constraints of discretized data

In practice, discretized values of the $F_I\left(\frac{a}{T}, \frac{a}{c}\right)$ factor of the stress intensity factor at the nodes of the mesh are given. Therefore, in order to take into account it, it is required that the first node value associated with a node n is equal to the $F_I\left(\frac{a}{T}, \frac{a}{c}\right)$ factor of this node. This nodal value will never change during iterations of the algorithm.

Now our definition of gradient vector and Hessian matrix can be justified. These are constructed from derivatives relatively to the nodal values except those that match the $F_I\left(\frac{a}{T}, \frac{a}{c}\right)$ factor at nodes (those we have set here actually). Now, it can be understood why these particular nodal values no longer vary in the algorithm and can no longer be considered as variables. Express a derivative with respect to these nodal values would therefore have no relevance.

3.3 Optimization algorithm

The smoothing optimization algorithm uses a Newton coupled to a linear search method. This is described below:

Algorithm:

Initialization: Equalize the concerned nodal values with those of the discretized $F_I\left(\frac{a}{T}, \frac{a}{c}\right)$ factor. Initialize other nodal values at 10^{-3} .

Until the arrest criterion is not reached, do:

a) Find the search direction \underline{d}_k with

$$\mathbf{H}\left(J(\underline{U}_k)\right) \cdot \underline{d}_k = -\mathbf{Grad}\left(J(\underline{U}_k)\right)$$

b) Find α_k which minimizes

$\Phi(\alpha_k) = J(\underline{U}_k + \alpha_k \cdot \underline{d}_k)$ (the linear search step)

c) Compute $\underline{U}_{k+1} = \underline{U}_k + \alpha_k \cdot \underline{d}_k$

\underline{U}_k is the vector encompassing all nodal values at the k th iteration of the algorithm. $\mathbf{H}\left(J(\underline{U}_k)\right)$ and $\mathbf{Grad}\left(J(\underline{U}_k)\right)$ are, respectively, the Hessian

matrix and the gradient vector associated with the functional to minimize at the k th iteration.

4 A method to move from virtual to real representation

4.1 Introduction

Earlier the discretized values in $\frac{a}{T}$ and $\frac{a}{c}$ for which the $F_I\left(\frac{a}{T}, \frac{a}{c}\right)$ factor was obtained numerically by finite element method had been presented. These discretized coordinate values are the same for both forms of study (semi-elliptical and quarter-elliptical crack):

$$\begin{cases} \frac{a}{T} \in \{0,1; 0,2; 0,4; 0,6; 0,8\} \\ \frac{a}{c} \in \{0,1; 0,2; 0,4; 0,6; 0,8;\} \\ \quad \quad \quad \{1; 1,2; 1,5; 2; 5; 10\} \end{cases} \quad (10)$$

Now, to avoid some numerical instabilities, one solution is to determine the smoothing on virtual coordinates that lead to identical dimensions elements:

$$\begin{cases} \frac{a}{T}^{virtual} \in \{1; 2; 3; 4; 5\} \\ \frac{a}{c}^{virtual} \in \{1; 2; 3; 4; 5; 6;\} \\ \quad \quad \quad \{7; 8; 9; 10; 11\} \end{cases} \quad (11)$$

A method to move from virtual coordinates to real coordinates without degrading regularity of the smoothing will be given in the next.

4.2 Solution of the problem

4.2.1 Definition of the metrics

To simplify the notation, the following associations will be made: $x = \frac{a}{T}^{virtual}$, $X = \frac{a}{T}$, $y = \frac{a}{c}^{virtual}$, $Y = \frac{a}{c}$. The resolution of the problem needs the introduction and determination of metrics characterizing the problem:

$$\begin{cases} dX = f(x) \cdot dx \Rightarrow \frac{dX}{dx} = f(x) \\ dY = g(y) \cdot dy \Rightarrow \frac{dY}{dy} = g(y) \end{cases} \quad (12)$$

For the regularity of a smoothing to be preserved, it is necessary that the two functions introduced either are continuous with the first derivative continuous also. To reuse what's already been done, the one-dimensional shape functions presented previously is used. More

specifically, these functions serve to represent the primitive of $f(x)$ and $g(y)$, respectively, $F(x)$ and $G(y)$.

Thus, in the j^{th} element:

$$\left\{ \begin{array}{l} z = \frac{x - x^{j+1}}{x^{j+1} - x^j} + \frac{x - x^j}{x^{j+1} - x^j} \\ F^j(z) = \begin{pmatrix} F_{11}^j \cdot C_{1,1}(z) + F_{12}^j \cdot C_{1,2}(z) \\ + F_{13}^j \cdot C_{1,3}(z) + F_{11}^{j+1} \cdot C_{2,1}(z) \\ + F_{12}^{j+1} \cdot C_{2,2}(z) + F_{13}^{j+1} \cdot C_{2,3}(z) \end{pmatrix} \\ F(x) = F^j(z) \end{array} \right. \quad (13)$$

$$\left\{ \begin{array}{l} z = \frac{x - x^{j+1}}{x^{j+1} - x^j} + \frac{x - x^j}{x^{j+1} - x^j} \\ G^j(z') = \begin{pmatrix} G_{11}^j \cdot C_{1,1}(z') + G_{12}^j \cdot C_{1,2}(z') \\ + G_{13}^j \cdot C_{1,3}(z') + G_{11}^{j+1} \cdot C_{2,1}(z') \\ + G_{12}^{j+1} \cdot C_{2,2}(z') + G_{13}^{j+1} \cdot C_{2,3}(z') \end{pmatrix} \\ G(x) = G^j(z') \end{array} \right. \quad (14)$$

To determine the unknown parameters of the metrics in each item uniquely, some relationships have to be determined. The goal is to have one relationship between the two representations so that there is no gain or loss of information.

4.2.2 Metrics compatibility with scales of the real and virtual elements

To simply understand the validity of these relationships, the reader can rely on the following figure.

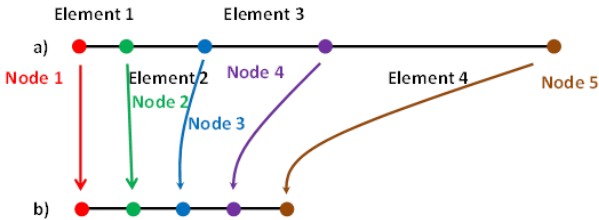


Fig. 7. Example of 1D mesh:
a) mesh in the real space,
b) mesh in the virtual space.

Only the equations on the function $F(x)$ will be presented. Those on $G(y)$ are deduced by analogy with the same approach.

The first equation to satisfy concerns the position of the **node 1**:

$$F(x^1) = F^1(z(x^1)) = X^1 \quad (15)$$

The properties of the shape functions, lead to $F_{11}^1 = X^1$.

It is possible to prove the following formulas by simple deduction for a mesh with N elements:

$$\begin{cases} F(x^j) = F^j(z(x^j)) = F^{j-1}(z(x^j)), \text{ for } j \in \llbracket 1; N \rrbracket \\ = F_{11}^j = F_{21}^{j-1} = X^j \\ F(x^j) = F^{j-1}(z(x^j)) = F_{21}^{j-1} = X^j, \text{ for } j = N + 1 \end{cases} \quad (16)$$

4.2.3 Minimization of curvature energy on the degrees of freedom to be determined

The previous equations can reduce the number of degrees of freedom and allow the correspondence between the nodes of real-dimensional mesh and those of the virtual mesh. Nevertheless, it remains to identify a bijective relationship between the two representations for points between nodes.

By analogy with what was presented in the previous section, the functional to minimize is (if the mesh consists of $n-1$ element):

$$W_x = \int_{x_1}^{x_n} \sqrt{(1 + (f(u))^2)} \cdot (\kappa(u))^2 \cdot du \quad (17)$$

Solving this optimization problem will be analogous to what was proposed in the previous sections.

5 Results

Some results are shown in the following figures. The case of a quarter-elliptical crack loaded with a uniform stress field and the $F_I\left(\frac{a}{T}, \frac{a}{c}\right)$ factor corresponds to the point c is considered. On the left figure it is shown that gives a classic linear interpolation between finite element results. Right, the same input data is used but the smoothing corresponds to the method presented in this article. The result is much smoother.

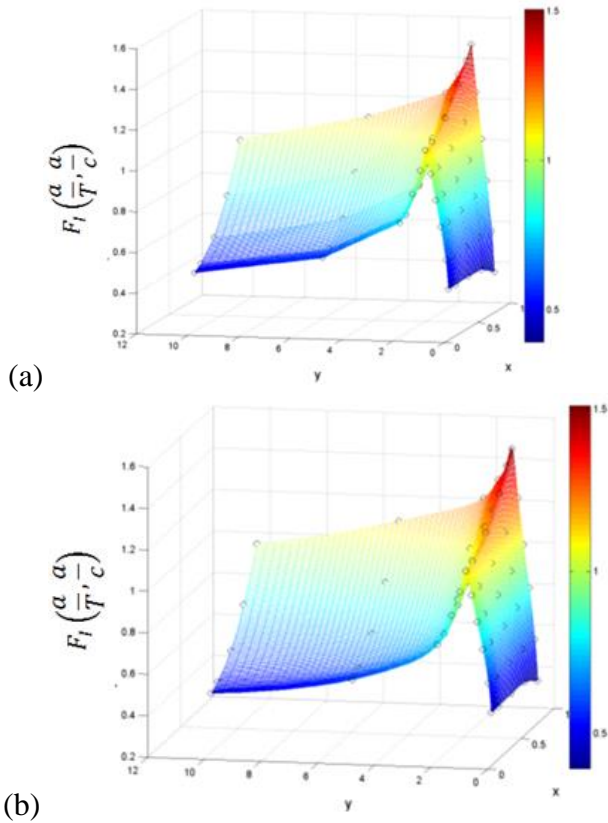


Fig. 8. Interpolation of the $F_I\left(\frac{a}{T}, \frac{a}{c}\right)$ factor:
 (a) linear interpolation,
 (b) the present methodology.

The figure below shows the differences between the two kinds of smoothing. The latter may reach 5% in this example and this impact with the same order of magnitude the stress intensity factor. And we therefore highlight the fundamental role of smoothing in the context of the life computed in crack propagation. While smoothing impact the stress intensity factor, it will impact inevitably the life computed.

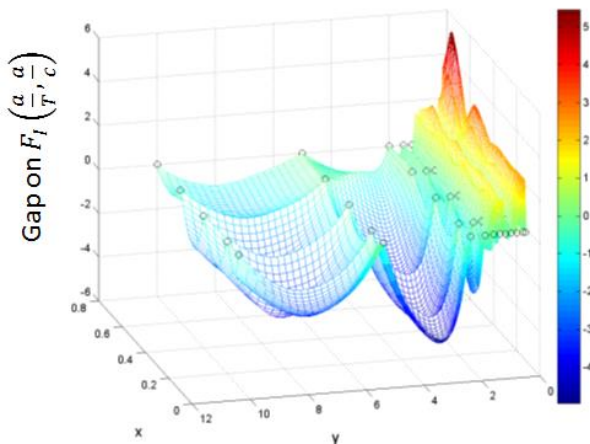


Fig. 9. Gap field between the two methods.

6 Conclusions

The method proposed should not be seen as a way to restore the stress intensity factor accurately. It is only a smoothing proposal which nevertheless seems more natural and physical than linear interpolation.

References

- [1] Rice J.R. A novel principle for the computation of stress intensity factors. *Angew. Math. Mech*, Vol. 50, pp 529-546, 1970.
- [2] Rice J.R. Some remarks on elastic crack-tip stress fields, *Int. J. Solids and Structures*, Vol. 8, pp 751-758, 1972.
- [3] Rice J.R. Weight function theory for three-dimensional elastic crack analysis, *Fracture Mechanics: Perspectives and Directions (Twentieth Symposium)*, ASTM STP 1020, R.P. Wei and R.P. Gangloff, Eds., American Society for Testing and Materials, Philadelphia, pp 29-57, 1989
- [4] Yu F. Construction of C2Q5 and C2Q7 Finite Elements on 2D Rectangular Meshes, *Master Thesis in Mathematics*, North Carolina State University, 2012.

Copyright Statement

The authors confirm that they, and/or their company or organization, hold copyright on all of the original material included in this paper. The authors also confirm that they have obtained permission, from the copyright holder of any third party material included in this paper, to publish it as part of their paper. The authors confirm that they give permission, or have obtained permission from the copyright holder of this paper, for the publication and distribution of this paper as part of the ICAS proceedings or as individual off-prints from the proceedings.